The Role of Bamboo Nanoparticles in Kenaf Fiber Reinforced Unsaturated Polyester Composites

Enih Rosamah[1], Abdul Khalil H.P.S.[2]*, S.W. Yap[2], Chaturbhuj K. Saurabh[2], Paridah M. Tahir[3], Rudi Dungani[4] and Abdulwahab F. Owolabi[2]

[1]*Faculty of Forestry, Mulawarman University, Campus Gunung Kelua, Samarinda 75119, East Kalimantan, Indonesia*
[2]*School of Industrial Technology, Universiti Sains Malaysia, 11800 Penang, Malaysia*
[3]*Laboratory of Biocomposite Technology, Institute of Tropical Forestry & Forest Products, Universiti Putra Malaysia, 43400 Serdang, Malaysia*
[4]*School of Life Sciences and Technology, Gandung Labtex XI, Institut Teknologi Bandung, Bandung 40132, Indonesia*

Received March 14, 2016; Accepted June 19, 2017

ABSTRACT: In this study, bamboo nanoparticles in concentration ranges from 0–5% were incorporated along with woven/nonwoven kenaf fiber mat into unsaturated polyester and the developed composites were further characterized. Bamboo chips were subjected to ball milling process for the synthesis of nanoparticles with a particle size of 52.92 nm. The effect that the incorporation of nanoparticles had on various properties of reinforced composites was further observed. Due to the high surface area of nanoparticles, incorporation of 3% of nanofillers contributed towards strong bonding and better wettability with matrix, thus resulting in excellent mechanical properties and thermal characteristics in reinforced unsaturated polyester composites. Furthermore, mechanical characteristics of reinforced composites were deteriorated by the addition of a higher percentage of nanoparticles (>3%) due to agglomeration, as confirmed by scanning electron microscopy. Moreover, ordered structural arrangement of woven kenaf textile fiber showed enhancement in interfacial adhesion and promoted superior mechanical strength in reinforced composites as compared with nonwoven composites.

KEYWORDS: Bamboo nanoparticles, kenaf fiber, reinforced composites, fatigue life, mechanical properties, thermal properties

1 INTRODUCTION

Polymer matrix having one or more dimension of at least one constituent less than 100 nm are best known as polymer nanocomposites. Incorporation of nanoparticles in a low percentage (1–5 wt% of polymer matrix) enhanced mechanical, barrier and thermal properties of nanocomposites as compared to pure polymer-based materials [1]. High surface area of nanoparticles assists in better adhesion and wettability with the matrix, thus improvements in various properties of nanocomposites are observed upon their incorporation in lower concentration. Furthermore, a lower concentration of nanoparticles helps in avoiding their agglomeration, as it is well known that formation of clumps could result in poor properties of composites. In the composite material, nanofillers show characteristics superior to those of traditional micro fillers in terms of better oxidation resistance, high optical transparency, and low permeability. On the basis of these characteristics, nanoparticles have become a hot spot in automotive, coating, and flame retardant applications [2]. With global awareness of the environment, renewable nanofibers as reinforcement in biocomposites are promoted as an alternative to synthetic fibers to achieve better sustainability and eco-efficiency. Fibers derived from renewable resources have many advantages over their synthetic counterparts, including low cost, low density, recyclability, biodegradability, abundance, and sustainability. Owing to such properties, natural fibers are interesting for further investigation [3].

Bamboo grows abundantly in tropical countries, specifically in Asia. Lakkad and Patel [4] stated that bamboo fiber has high mechanical properties in terms of ultimate tensile, toughness, and Young's modulus

*Corresponding author: akhalilhps@gmail.com

DOI: 10.7569/JRM.2017.634152

 DOI: 10.7569/JRM.2017.634152

that fulfill the requirements of an ideal natural filler in the nanocomposite material, having structural applications such as in construction. Moreover, bamboo, also called 'natural glass fiber,' is known for its relatively high strength over weight owing to the longitudinal alignment of fiber structure in its body [5]. Kenaf is also a promising natural fiber as reinforcement material to fabricate composite due to its distinctive features, including its high mechanical strength, renewability, low density, and environmental friendliness [6]. To enhance mechanical interlocking of reinforcement, its geometrical modification can be carried out through weaving to improve interfacial adhesion and strength of composites. Several studies have been conducted in the past to compare the effect of woven and unidirectional structural arrangement of fibers on the mechanical, morphological, and physical properties of composites [7–9].

The addition of organic nanoparticles as filler and rearrangement of the textile structure of reinforced composites have been studied separately. However, no study has been done yet considering both parameters in one composite material. The incorporation of oil palm shell nanoparticles [10, 11] and rearrangement of the textile structure of kenaf reinforced unsaturated polyester [12, 13] have been studied in the past. These studies reported that both nanoparticles incorporation as filler and weave designed kenaf mat significantly improved the properties of composites to the extent that it can be of potential use in various industries, including the construction and automotive industries. Thus, the main aim of the present study is to investigate the effect of incorporation of bamboo nanoparticles on woven/nonwoven kenaf fiber mat reinforced unsaturated polyester resin matrix.

2 EXPERIMENTAL

2.1 Preparation of Bamboo Nanoparticles

Bamboo (*Bambusa blumeana*) was obtained from a forest located in Ulu Kechil Hilir, Kedah, Malaysia. The bamboo culms were cut into slices approximately 15 cm long and chipped through a hammer mill. Bamboo chips were crushed and ground using a grinding machine (model WRB 90Lb/4P, Dietz-Motoren GmbH & Co., Dettingen, Germany). Powdered bamboo was then screened through a 60 mesh size sieve to obtain micro size with the help of a Retsch 3D shaker. The sample was dried at 105 °C for 24 h to remove moisture. The sample was then sieved using 20 µm size mesh and further ground using the same grinding machine three more times. Obtained sample was then treated by a high energy ball mill equipped with a 0.5 L mild steel ball mill pot having stainless steel balls of different sizes and rotated at a speed of 175 rpm for 120 h. Obtained nanoparticles were then dried in an oven at 110 °C for 24 h to remove moisture and immediately stored in a desiccator until further use.

2.2 Analysis of Bamboo Nanoparticles

Structure and morphology of bamboo nanoparticles were determined by transmission electron microscopy (TEM) using a Philips CM 12 instrument (Germany). The sample was diluted to 2 mg/mL with ethanol and placed in an ultrasonicator for 10 min. A tiny drop of the colloidal dispersion of sample was carefully placed on a carbon-coated copper grid and dried at room temperature prior to examination using TEM. Particle size distribution of nanoparticles was identified with dynamic light scattering method using Malvern Zetasizer Ver. 6.11 (MAL 1029406, Germany) equipped with a laser having a wavelength of 532 nm. The sample was dispersed in distilled water and placed in the ultrasonic bath for 6 min prior to analysis. Each sample was analyzed in triplicate. The XRD pattern of the sample was identified using a Philips PW1050 X-Pert diffractometer equipped with CuKα radiation (λ = 1.54 Å) at 40 kV. Diffractograms were recorded from 7°–80° (2θ) in steps of 0.02° with a scanning rate of 0.5°/min. The relative crystallinity index (CI) was calculated using peak height method:

$$CI(\%) = \frac{(I_{002} - I_{am})}{I_{002}} \times 100$$

where I_{002} and I_{am} are the peak intensity corresponding to crystalline and amorphous fraction respectively.

2.3 Composite Fabrication

Matrix phase was prepared by mixing polyester resin (60 wt% of total composition) with different nanoparticle filler loadings (as shown in Table 1) and 2% (w/w of resin) of methyl ethyl ketone peroxide (MEKP) as a catalyst. The solution was further mixed by a mechanical stirrer at a speed of 1000 rpm for 10 min. The obtained formulation was then vacuumed in a chamber to remove air bubbles. Further, the resin mixture was casted on woven or nonwoven kenaf fiber mat (40 wt% of total composition) having a dimension of 204 mm × 204 mm × 50 mm using hand layup process. Samples were left to cure in a cold press at 200 psi for 24 h. Polymerization occurred during post cure in an oven at 105 °C. The appearance of all fabricated samples was similar to those displayed in Figure 1 and they were coded and prepared according to Table 1.

2.4 Characterization of Nanofiller Reinforced Fiber Composites

The density of composites was measured as per ASTM D2395-14 standard. Void content of composites was determined according to ASTM D2734 standard. Absorption capacity was observed by immersing samples in distilled water at ambient temperature. Water absorption rate was calculated as per ASTM D570 standard. All experiments were repeated five times to obtain a mean value for each sample.

Tensile properties of composites were studied based on ASTM D3039 using an Instron model 5582 100kN Universal Testing Machine. The testing speed was controlled at 5 mm/min and gauge length was fixed at 60 mm. The flexural test was carried out according to ASTM D790-03 specification. For three-point bending test, crosshead speed was fixed at 2 mm/min and a distance of 90 mm between both the supporters was set. Izod notched impact test was carried out using a Geotech testing machine (model GT-7045 MD) according to ASTM D256-2006. Each composite was cut to the dimension of 70 mm × 15 mm × 5 mm using a circular saw. Specimens were placed into the impact tester with a notch cut in one side. Fatigue life of the composites was investigated with a 100kN capacity Universal Testing Machine as per ASTM D3479 method. Samples were sanded at the edges and bonded with 1 mm thick aluminum tab using hot-melt adhesive (silicon glue gun) to reduce slippage when loads were applied during the test. Testing was conducted with tension-tension fatigue loading under constant stress. The R ratio was fixed at 0.5 at three stress levels loaded cyclically at 50%, 70%, and 90% of its ultimate tensile strength. The condition was fixed at 5Hz tensile frequency and 20 °C. For all experiments, each sample was replicated five times and a mean reading of all data was calculated.

Scanning electron microscopy was used to investigate the morphology of samples. The fractured surface of the composite during the flexural test was observed using an electron microscope (Leo Supra 50 VP, Carl Zeiss SMT, Germany). The sample was sputtered with gold prior to observation at 5kV acceleration. Thermal stability was determined by a PerkinElmer Pyris I thermogravimetric analyzer (PerkinElmer, USA). The specimen was ground into powder prior to analysis. Thermal analysis was conducted at a temperature range from 30 °C to 800 °C with 20 °C per minute heating rate under nitrogen atmosphere.

Table 1 Coding and parameters of composites manufactured.

Nanoparticles filler loading content (wt% of total composite)	Woven (WRC)	Nonwoven (NWRC)
0	W0	NW0
1	W1	NW1
2	W2	NW2
3	W3	NW3
4	W4	NW4
5	W5	NW5

3 RESULTS AND DISCUSSION

3.1 Characterization of Bamboo Nanoparticles

A TEM image of agglomerated bamboo nanoparticles is shown in Figure 2a. When primary particles agglomerate they formed a structure called secondary particles,

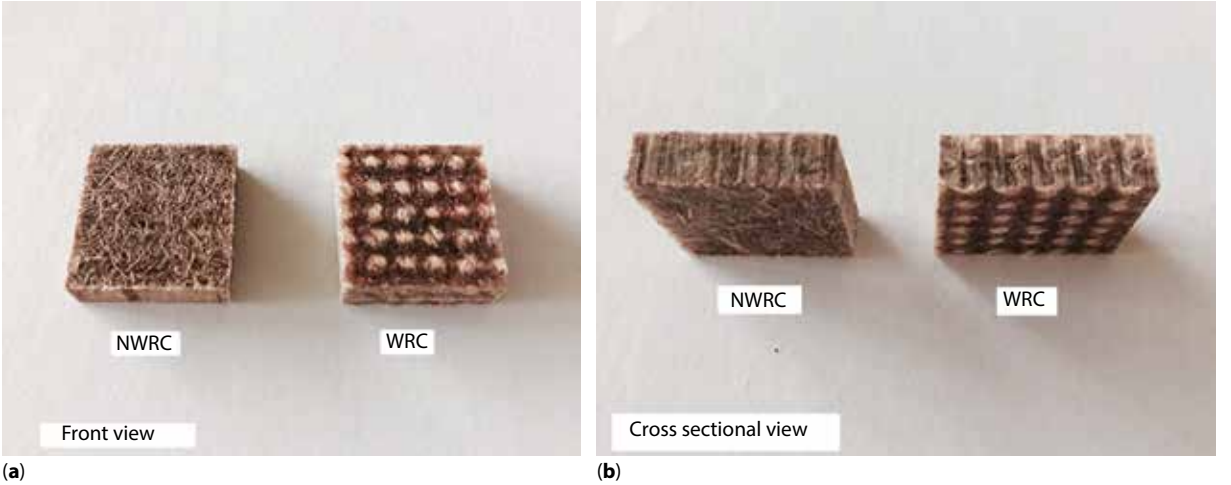

Figure 1 nonwoven reinforced composite (NWRC) and woven reinforced composite (WRC): (**a**) front view, (**b**) cross sectional view.

 DOI: 10.7569/JRM.2017.634152

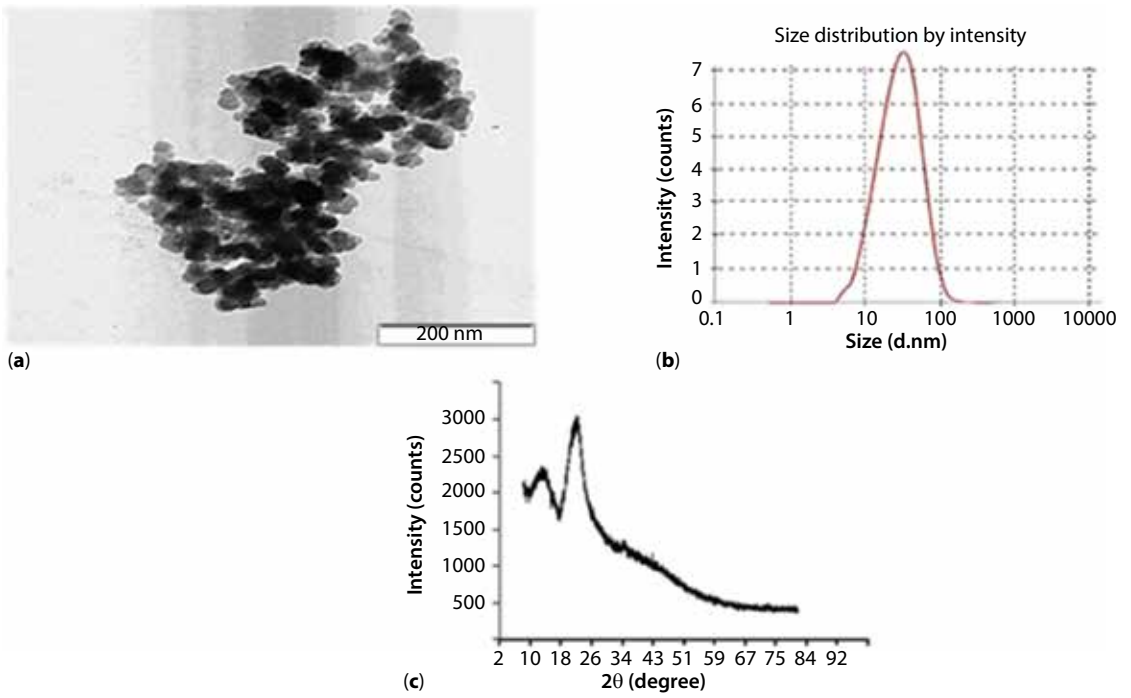

Figure 2 Bamboo nanoparticles: (**a**) TEM micrograph, (**b**) size distribution by intensity and (**c**) X-ray diffractogram.

which are held by weak intermolecular forces or chemical bonds [14]. The average size of obtained nanoparticles was 52.92 nm, as observed by particle size analyzer. Figure 2b shows particle size distribution of nanoparticles, which ranged from 5.9 nm to 122.4 nm. However, the size range from 5.9 nm to 99.96 nm covered 98.6% of total intensity. Generally, most of the biomass materials exhibit strongest diffraction peak and relatively high crystallinity due to their morphological structures [15]. In this study, the presence of noncellulosic contents in bamboo fiber resulted in significant amorphous and crystalline diffraction peak areas. As seen in the XRD spectrum in Figure 2c, the relative crystallinity of bamboo nanoparticles was 44.76%. This denoted that the particle size of bamboo was changed during milling without altering the chemical structure, thus retaining its crystallinity. A similar result was observed for the untreated raw bamboo particle in a previous study [16] that exhibited crystallinity of 44.4%. Yueping *et al.* [17] stated that bamboo fiber has tremendous potential to produce high mechanical strength composite due to its crystalline structure.

3.2 Physical Properties of Nanoparticles Reinforced in Kenaf-Based Composites

Table 2 shows the experimental and theoretical density of samples. Densities of reinforced composite were directly proportional with the increment of nanofiller content. Table 2 highlights that W5 exhibited the highest measured and theoretical densities overall results compared with others, which were 1.195 ± 0.05 g/cm^3 and 1.255 ± 0.07 g/cm^3. It can be seen that WRC had higher densities compared with NWRC samples. This has been explained by the fact that woven fabric has a more compact structure of fibrils providing more sites for bonding with matrices, which results in less void and subsequently high density [18]. According to Table 2, for all samples theoretical density was higher than measured density, which could be explained by the presence of voids in composites.

Unfilled composites had highest void contents (NW0 = 2.5 ± 0.54%, W0 = 4.78 ± 0.08%), whereas, both NW3 and W3 exhibit least void content of 1.01 ± 0.01% and 2.84 ± 0.06%, respectively, among all samples. This indicated the homogeneous dispersion of nanoparticles in composites and this phenomenon further assisted the nanoparticles in replacing voids present in the composite [19]. A high percentage of voids were observed in samples when more than 3% of nanoparticles was incorporated into the samples. This effect might be due to the agglomeration of particles during mixing with resin, which further caused inhomogeneous dispersion of the filler in the matrix, thus resulting in void formation. Besides that, Table 2 also highlights that WRC had more voids compared with NWRC. This might be due to the fact that more

Table 2 Measured density, theoretical density and void content of woven and nonwoven composites.

Samples	Coding	Measured density (g/cm³)	Theoretical density (g/cm³)	Void content (%)
Nonwoven	NW0	1.138 ± 0.02	1.157 ± 0.07	2.50 ± 0.54
	NW1	1.144 ± 0.02	1.161 ± 0.03	1.11± 0.04
	NW2	1.148 ± 0.01	1.164 ± 0.09	1.09 ± 0.09
	NW3	1.153 ± 0.02	1.169 ± 0.04	1.01 ± 0.01
	NW4	1.159 ± 0.06	1.172 ± 0.03	1.25 ± 0.09
	NW5	1.172 ± 0.05	1.202 ± 0.07	1.64 ± 0.04
Woven	W0	1.175 ± 0.06	1.215 ± 0.07	4.78 ± 0.08
	W1	1.178 ± 0.03	1.217 ± 0.03	3.02 ± 0.09
	W2	1.183 ± 0.06	1.219 ± 0.08	2.91 ± 0.07
	W3	1.186 ± 0.09	1.222 ± 0.03	2.84 ± 0.06
	W4	1.189 ± 0.08	1.226 ± 0.06	3.11 ± 0.08
	W5	1.195 ± 0.05	1.255 ± 0.07	3.29 ± 0.07

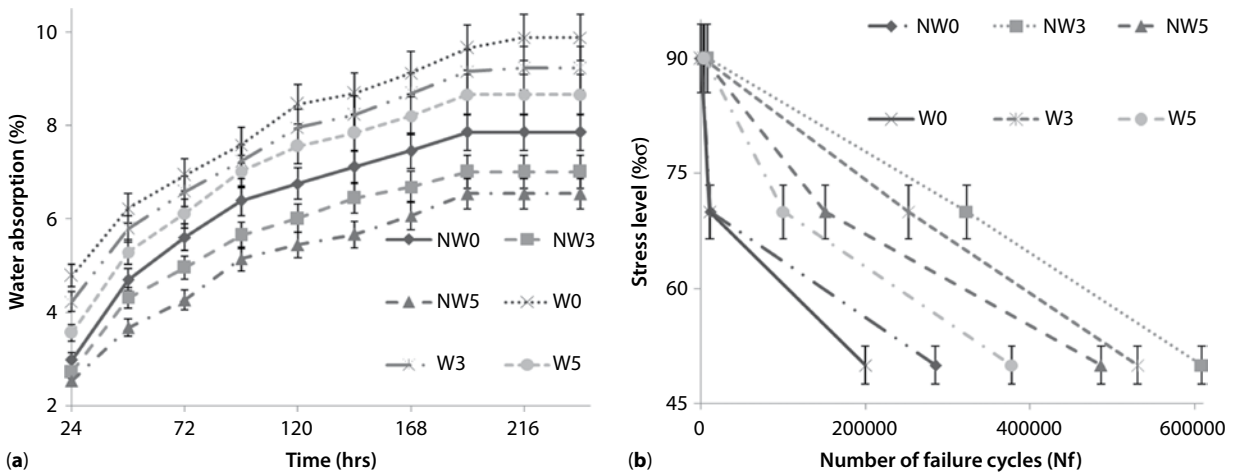

Figure 3 Nanoparticles incorporated woven/nonwoven reinforced composites' (**a**) water absorption properties, (**b**) relation between stress level and number of failure cycles.

air inclusion occurs in woven kenaf. The inability of woven fiber to eliminate all air bubbles trapped inside also resulted in high void content [20]. High void content in composites significantly affects its mechanical strength [8].

Water absorption of reinforced composite is affected by various factors, including temperature, fiber orientation, diffusibility, and degree of surface exposure. It can be observed through Figure 3a that the water absorption rate increased with soaking time up to 192 h; thereafter the rate remained constant. Water absorption capacity of WRC was higher than NWRC. This was due to the high porosity of WRC because of the presence of voids; thus more water was trapped and resulted in higher weight gain of the composite. Unfilled WRC exhibited highest water absorption value due to the high void percentage, as observed in Table 2, and this has led to poor wettability and weak adhesion interface between fiber and matrix. Furthermore, it was observed that percentage of water absorption decreased with concentration of nanoparticles. This denoted that the nanoparticle content increased the water resistance of composites due to the high surface contact area of nanoparticles, which allows stronger adhesion interface bonding and better wettability with the matrix. Rana [21] stated that nanoparticles have the ability to trap water molecules and thus hinder moisture diffusion in composites

and maintain its structure. Similar results were also reported in many previous studies [22, 23].

3.3 Mechanical Properties

Tensile modulus, tensile strength, and elongation at break were analyzed in the present study with the stress-strain curve. Obtained data are presented in Table 3. The tensile strength of both WRC and NWRC increased with filler content up to 3% and decreased thereafter. Highest tensile strength was obtained for NW3 having a value of 39.23 ± 1.19 MPa and for W3 it was 55.68 ± 1.74 MPa. Several studies have proven that low filler loading is able to enhance the tensile strength of composites, attributed to strong hydrogen bonding between fiber and matrix [24]. At 5% of nanoparticles filler, NW5 and W5 demonstrated a reduction in tensile strength to a value of 30.49 ± 0.94 MPa and 34.66 ± 0.54 MPa, respectively. Osman *et al.* [25] suggested that excess of filler content led to the formation of agglomerate, which resulted in poor adhesion between filler and matrix, thus weakening the tensile strength of composites. Table 3 also shows that WRC had higher tensile strength than NWRC, indicating that the applied tensile stress was able to propagate evenly within the compact and jammed structure of woven kenaf. The interlocking structure of woven fabric has restrained the mobility within it and this could be advantageous in fully utilizing the strength of fiber [26].

Tensile modulus also exhibited similar trends as the data of tensile strength. Reinforced composites with 3% of nanoparticles showed highest tensile modulus (NW3 = 1.19 ± 0.41 GPa, W3 = 1.93 ± 0.32 GPa). The uniform dispersion of nanoparticle filler into unsaturated polyester matrix resulted in enhanced rigidity and stiffness of composites. Devaprakasam *et al.* [27] stated that filler particles help in energy dissipation and thus resulted in improved tensile modulus. Both WRC and NWRC with filler content above 3% have shown poor tensile modulus. A similar issue was also reported by Chandradass *et al.* [28] in their study. Abdul Khalil *et al.* [29] stated that inhomogeneity of fiber/matrix dispersion will disturb the effectiveness of load propagation within fibers and weaken mechanical properties of composites. WRC exhibits higher tensile modulus when compared with NWRC. The compact structure of weave orientated fiber mat gave composites a stiffer structure and strong resistance to withstand an applied load.

Reduction in elongation at break was inversely proportional to filler concentration in reinforced composites. The nanoparticles concentration-dependent decrease in % elongation was observed for all composites. At 5% of nanoparticles lowest elongation at break was observed. The NW5 demonstrated a value of 7.86 ± 1.24% and W5 showed a value of 6.02 ± 0.42%. There are several factors related to inelasticity of composites. Higher concentration of nanoparticles has contributed to early fracture and deformation of composites [30]. The aggregation of nanoparticles allowed stress concentration area to form and such weak regions can lead to an early crack in reinforced composites even when only a little stress is applied. The previous study also showed similar results [31]. All WRC showed lower elongation at break than NWRC in this study.

Table 3 Mechanical properties of woven and nonwoven kenaf fiber reinforced unsaturated polyesters with different bamboo nanoparticles filler concentration.

Composite	Tensile strength (MPa)	Tensile modulus (GPa)	% Elongation at break	Flexural strength (MPa)	Flexural modulus (GPa)	Impact strength (kJ/m²)
NW0	30.32 ± 0.51	1.03 ± 0.06	8.97 ± 1.16	50.8 ± 1.29	2.54 ± 0.16	3.56 ± 0.23
NW1	34.66 ± 0.64	1.12 ± 0.05	8.95 ± 0.04	55.3 ± 0.20	3.30 ± 0.19	4.44 ± 0.29
NW2	36.12 ± 1.21	1.15 ± 0.03	8.68 ± 0.12	57.9 ± 1.19	3.71 ± 0.12	4.87 ± 0.39
NW3	39.23 ± 1.19	1.19 ± 0.04	8.47 ± 1.29	59.7 ± 2.32	3.99 ± 0.13	5.23 ± 0.43
NW4	35.38 ± 1.03	1.14 ± 0.07	8.09 ± 1.06	56.3 ± 1.98	3.18 ± 0.18	4.41 ± 0.32
NW5	30.49 ± 0.94	1.08 ± 0.09	7.86 ± 1.24	53.6 ± 0.52	2.60 ± 1.23	3.85 ± 0.23
W0	33.96 ± 0.35	1.54 ± 0.06	7.44 ± 0.38	67.9 ± 0.53	2.88 ± 0.12	5.85 ± 0.24
W1	49.46 ± 0.96	1.72 ± 0.03	6.97 ± 1.58	71.6 ± 1.23	3.66 ± 0.37	6.85 ± 0.36
W2	52.34 ± 1.22	1.84 ± 0.07	6.71 ± 0.63	72.6 ± 2.89	4.07 ± 0.42	7.19 ± 0.21
W3	55.68 ± 1.74	1.93 ± 0.03	6.55 ± 0.52	75.6 ± 1.98	4.65 ± 0.48	7.43 ± 0.32
W4	42.51 ± 1.89	1.87 ± 0.04	6.39 ± 0.47	64.1 ± 1.64	3.96 ± 0.37	6.68 ± 0.43
W5	34.66 ± 0.54	1.70 ± 0.06	6.02 ± 0.42	53.3 ± 0.67	3.03 ± 0.48	5.94 ± 0.94

The strong directional properties of a compact woven structure have promoted high stiffness in composites, thus resulted in a loss of elasticity.

The flexural properties of fiber mat are presented in Table 3. Reinforced composites with 3% of filler content exhibited highest flexural strength (NW3 = 59.7 ± 2.32 MPa, W3 = 75.6 ± 1.98 MPa). Bamboo nanoparticles have high contact surface area which contributed to strong interfacial bonding between filler and matrix and thus resulted in an even distribution of propagating stress when applied [34]. At filler loading upwards of 4%, reinforced composites demonstrated a decrease in flexural strength. Similar results were observed in many previous studies [32,33]. Mortazavi *et al.* [32] stated that the excess amount of nanoparticles resulted in the high viscosity of matrix and this led to an increased porosity which in turn affected the composite strength. As expected, WRC showed better flexural strength than NWRC and this was due to the intact strength of the weave pattern of the fiber mat. Alhuthali *et al.* [35] also observed a similar trend in the flexural strength of kenaf fiber reinforced composites.

Flexural modulus illustrated the same trend as the flexural strength of reinforced composites. Flexural modulus increased with filler loading till 3% and decreased thereafter for both WRC and NWRC (Table 3). The strong adhesional interface between filler-matrix promoted by uniform dispersion of a small amount of nanoparticles into reinforced composites controlled the elasticity of matrix [37]. The agglomeration of excess filler content (≥ 4%) resulted in a stress concentrated area that brings down flexural modulus of reinforced composites [35]. The continuous weave design of fiber mat formed a compact structure that can hold greater load than that of the nonwoven fiber mat-based composites. The stress concentration was propagated evenly within the fiber structure itself and this gave enhanced mechanical properties to WRC as compared to NWRC.

Table 3 shows impact strength of reinforced composites. A 3% concentration of filler in reinforced composites resulted in highest impact strength for both types of composites. The NW3 showed a value of 5.23 ± 0.93 kJ/m² and W3 demonstrated a value of 7.43 ± 0.72 kJ/m². The addition of a little amount of filler loading enhanced adhesion interface bonding between fiber and matrix phases and thus improved the toughness of composites. The excess of filler concentration at 4% and 5% resulted in agglomeration of nanoparticle filler in reinforced composite that affected its dispersion in matrix phase and caused incomplete wetting fabrication, which led to low impact strength [35]. Similar to tensile test, WRC exhibited higher impact strength than NWRC. Woven structure of WRC has an ability to absorb and propagate the force within the structure more efficiently than NWRC.

Fatigue life of reinforced composites can be identified under different levels of tension-tension cyclic stress. Figure 3b illustrates the relationship of cyclic stress and fatigue life of WRC and NWRC with different nanoparticle concentrations. The interfacial bonding between fiber and matrix of reinforced composites were affected when higher cyclic stress was applied. The results shown in Figure 3b prove that nanoparticle filler has the ability to inhibit fracture failures during low cyclic loading. Previously, Berhan *et al.* [37] stated that the fatigue life of 1 to 1×10^3 is classified as low cyclic fatigue, whereas, the high cycle fatigue is in between 1×10^3 to 1×10^6. Both reinforced composites with 3% nanoparticles exhibit the longest fatigue life as compared to their respective non-reinforced composite or reinforced composite. This was due to stronger interfacial adhesion between fiber and matrix which allowed stress to propagate within the constituents and contributed to the deceleration of fracture mechanism in reinforced composites. This resulted in a better capacity of the composite to withstand cyclic damages [38]. Whereas, 4% and 5% of nanoparticles in composites resulted in lower fatigue life under cyclic stress due to the agglomeration of filler particles. The relationship of stress-cycle (S-N) curve in Figure 3b shows that the WRC had lower fatigue life than the NWRC. Similar fatigue properties for woven and nonwoven glass fibers were previously reported by Loos *et al.* [38]. Fatigue behavior of woven composites was made up of three stages. Microcrack formation on weave is an initial stage which leads to the reduction of modulus due to stress concentration. Shear failures at warp and cracks at matrix begin in the middle stage and, finally, failure modes occur during the last stage [40].

3.4 Morphological Properties

Scanning electron microscopy (SEM) images of the fracture surface of reinforced composites with different nanoparticle filler content and mat structure is illustrated in Figure 4 at 1000× magnification. The fracture behavior of reinforced composites is related to fracture surface roughness [41]. It was observed in Figure 4a and 4b that unfilled reinforced composites had a smooth fractured surface as compared to composite filled with nanoparticles. Microcracks that can be seen in SEM micrographs were initiated by the non-homogeneity of reinforced composites [42]. At 3% of nanoparticles, more cracks appeared as compared to unfilled reinforced composites (Figure 4c,d). This was due to the uniform dispersion of nanoparticles in matrix, which resulted in strong interface adhesion

 DOI: 10.7569/JRM.2017.634152

and higher strength for composite. Figure 4e and 4f with 5% of filler concentration demonstrated agglomerations of nanoparticles on the fractured surface. This has led to microcracks at the matrix site due to weak interfacial adhesion bonding between fiber and matrix because of the non-homogeneous dispersion of the filler. Poor interface adhesion has led to inferior stress transfer within the composite [25].

The SEM micrographs in Figure 5 illustrate the surface morphology of reinforced composites at a magnification of 300×. Figure 5a and 5b show fiber detachments in both unfilled NWRC and WRC, respectively. Samples had more obvious fiber pull-off due to the failure of interfacial adhesion within kenaf fiber and unsaturated polyester matrix. Whereas, an addition of 3% of bamboo nanoparticles contributed to improved bonding between fiber and matrix, which resulted in embedded fiber breakage instead of fiber pull-out (Figure 5c,d). Lenz and dos Santos [43] also suggested that more fiber breakage occurred in fiber reinforced composites with addition of nanoparticle filler when tension is applied. Higher fiber tearing denoted that the bonding within fiber and matrix is strong. It can be observed from Figure 5e and 5f that the aggregation of bamboo nanoparticles at 5% around the interface between fiber and polymer matrix occurred. This led to microcracks, as seen on the fractured surface, and subsequent poor mechanical properties like tensile, flexural, impact, and fatigue properties of composites were observed.

3.5 Thermal Properties

Thermal stability and degradation of WRC and NWRC with different filler content were determined by thermogravimetric analysis. Figure 6 shows that the two stages of thermal degradation were observed for all samples. The weight loss of composites at an early

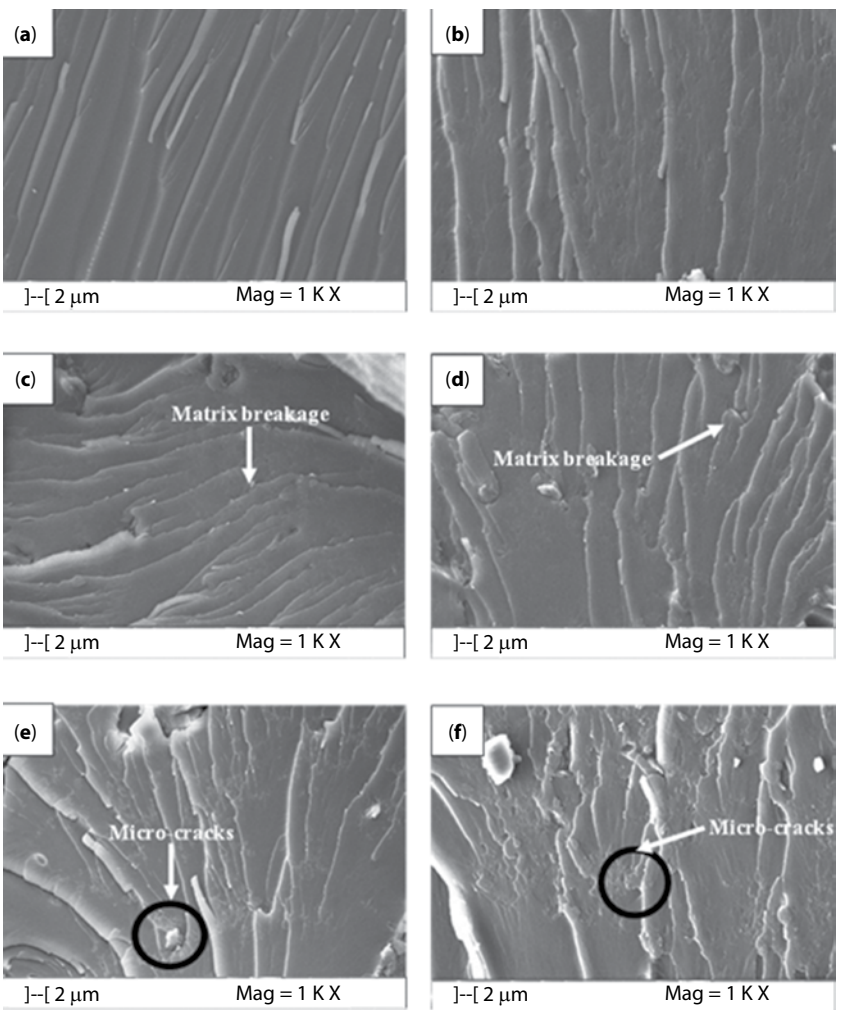

Figure 4 SEM micrographs (at magnification 1000×) of (**a**) NW0, (**b**) W0, (**c**) NW3, (**d**) W3, (**e**) NW5, and (**f**) W5.

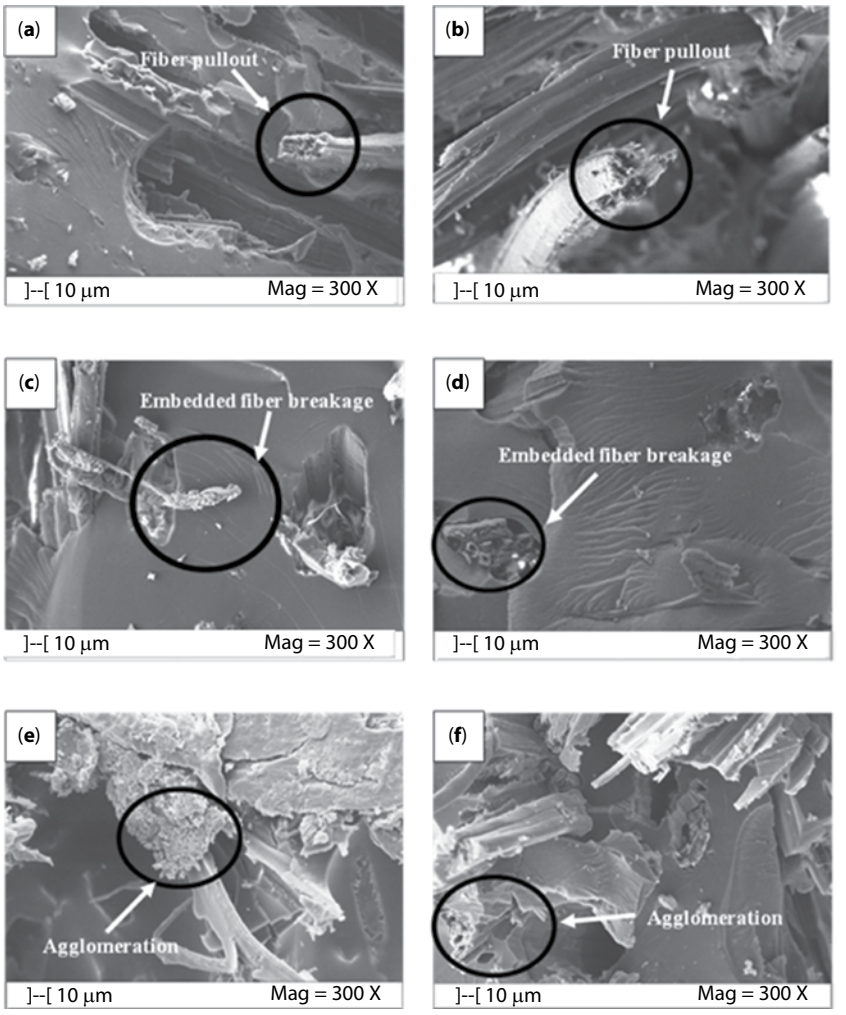

Figure 5 SEM micrographs (at magnification 300×) of (**a**) NW0, (**b**) W0, (**c**) NW3, (**d**) W3, (**e**) NW5, and (**f**) W5.

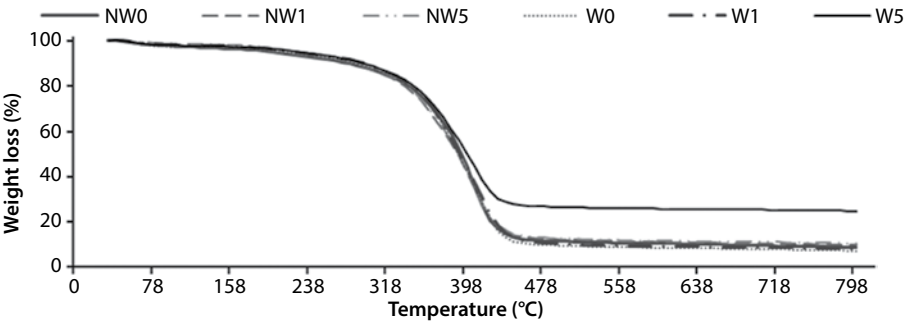

Figure 6 TGA thermograms of reinforced composites with different bamboo nanoparticles filler content.

stage around 90 °C to 100 °C denoted the removal of moisture [44]. It was observed that a low amount of nanoparticles incorporation up to 3% resulted in increased thermal stability of reinforced composites as compared to non-reinforced composites, as observed by the value of T_{max}, T_i, and T_f (Table 4). Thermal stability can be determined by the point where a material begins to disintegrate, which is also known as initial decomposition temperature [45]. Nanoparticle filler improved crosslinking and interfacial adhesion within

 DOI: 10.7569/JRM.2017.634152

Table 4 Degradation temperature and char residues of reinforced composites.

Composites	Degradation temperature (°C)			Char residue (%)
	(T_i)	(T_f)	(T_{max})	
NW0	255.53	403.80	353.75	8.67
NW1	262.98	405.59	363.53	9.92
NW2	265.89	406.33	367.86	10.18
NW3	268.71	407.97	369.45	10.27
NW4	264.52	406.16	361.27	10.41
NW5	259.82	405.48	355.43	10.53
W0	263.21	416.28	359.19	7.43
W1	300.85	419.50	373.78	8.06
W2	302.09	420.77	374.52	9.68
W3	305.64	422.61	377.48	11.29
W4	293.32	421.09	371.83	12.46
W5	282.55	418.24	367.43	13.79

fiber and matrix. Furthermore, uniform dispersion of nanoparticles in composites resulted in improved thermal properties [46]. Nanoparticles formed a heat shield in reinforced composites, thus inhibiting heat transfer and thermal degradation of polymers [47]. Table 4 also shows that the low thermal degradation resulted from the incorporation of nanoparticle filler concentration beyond 3%. This denoted that the agglomeration of nanoparticles failed to impose interfacial adhesion and molecular mobility, which led to weak thermal stability. The thermal degradation (T_{max}) of WRC ranged from 359.19 °C to 377.48 °C and was higher than NWRC, which ranged from 353.75 °C to 369.45 °C. The chemical crosslinking at interface resulted in a better formation of the network at an interface in woven composites, thus resulting in thermal stability. Furthermore, the non-volatile component that remained at 800 °C, also known as char residue, was also determined. The char residue increased with the increase in nanoparticle concentration due to higher inorganic content in composites.

4 CONCLUSION

Bamboo nanoparticles were produced by using ball milling process and their properties were characterized by particle analyzer, X-ray diffraction, and TEM. Obtained nanoparticles had a mean size of 52.92 nm and crystallinity index of 44.76%. The incorporation of bamboo nanoparticles enhanced the density of composites. Void content was lowered upon addition of 3% of nanoparticles but increased from 4% and beyond due to its agglomeration. Water absorption rate of reinforced composites is inversely proportional to bamboo nanoparticles concentration. The addition of a small amount of nanoparticles (up to 3%) improved the matrix-fiber interfacial bonding and enhanced the tensile strength and modulus, flexural strength and modulus, impact strength, fatigue life, and thermal stability of woven/nonwoven reinforced composites. Furthermore, the woven structure of kenaf fiber mat exhibited higher physical, morphological, mechanical, and thermal characteristics as compared to nonwoven samples due to its superior dimensional stability. However, fatigue life of woven reinforced composites is lower than nonwoven composite due to the unstable stress concentration on the structural pattern of woven fiber. Beyond 3% of nanoparticle filler concentration, all studied properties deteriorated in all samples due to the poor interfacial adhesion between fiber and matrix because of agglomeration of nanoparticles. Elongation at break shows a decline with an increase in nanoparticles loading at all concentrations. Overall, it can be concluded on the basis of obtained results that 3% of nanoparticle incorporation into woven kenaf fiber reinforced polyester composite had superior properties compared with all the studied samples.

ACKNOWLEDGMENTS

All authors are grateful to Universiti Sains Malaysia, Penang, Malaysia, for providing Research University Grant (RUI-1001/PTEKIND/814255). The authors are also grateful for the collaboration between Universiti Sains Malaysia, Penang, Malaysia, and Mulawarman University, Samarinda, East Kalimantan, Indonesia.

REFERENCES

1. P.M. Ajayan, L.S. Schadler, and P.V. Braun, *Nanocomposite Science and Technology*, Wiley-VCH, Weinheim (2006).
2. K.I. Winey and R.A. Vaia, Polymer nanocomposites. *MRS Bull.* **32**(4), 314–322 (2007).
3. F. Vilaplana, E. Strömberg, and S. Karlsson, Environmental and resource aspects of sustainable biocomposites. *Polym. Degrad. Stab.* **95**(11), 2147–2161 (2010).
4. S. Lakkad and J. Patel, Mechanical properties of bamboo, a natural composite. *Fibre Sci. Technol.* **14**(4), 319–322 (1981).
5. K. Okubo, T. Fujii, and Y. Yamamoto, Development of bamboo-based polymer composites and their mechanical properties. *Compos. Part A-Appl. S.* **35**(3), 377–383 (2004).
6. T. Nishino, K. Hirao, M. Kotera, K. Nakamae, and H. Inagaki, Kenaf reinforced biodegradable composite, *Compos. Sci. Technol.* **63**(9), 1281–1286 (2003).
7. J.L. Abot, A. Yasmin, A.J. Jacobsen, and I.M. Daniel, In-plane mechanical, thermal and viscoelastic properties of a satin fabric carbon/epoxy composite. *Compos. Sci. Technol.* **64**(2), 263–268 (2004).
8. M. Jawaid, H.A. Khalil, A.A. Bakar, and P.N. Khanam, Chemical resistance, void content and tensile properties of oil palm/jute fibre reinforced polymer hybrid composites. *Mater. Design* **32**(2), 1014–1019 (2011).
9. W. Lai, M. Mariatti, and S.M. Jani, The properties of woven kenaf and betel palm (*Areca catechu*) reinforced unsaturated polyester composites. *Polym-Plast. Technol.* **47**(12), 1193–1199 (2008).
10. W.N.B.W. Othman, Characterization of oil palm shell nanofiller in hybrid kenaf/coconut fibres reinforced polyester composites, MSc Thesis, Universiti Sains Malaysia (2014).
11. E. Rosamah, M.S. Hossain, H.P.S.A. Khalil, W.O.W. Nadirah, R. Dungani, A.S.N. Amiranajwa, N.L.M. Suraya, H.M. Fizree, and A.K.M. Omar, Properties enhancement using oil palm shell nanoparticles of fibers reinforced polyester hybrid composites. *Adv. Compos. Mater.* **26**(3), 259–272 (2017).
12. M. Saiman, M.S. Wahab, and M.U. Wahit, The effect of fabric weave on the tensile strength of woven kenaf reinforced unsaturated polyester composite, Paper presented at the Proceedings of the International Colloquium on Textile Engineering, Fashion, Apparel and Design 52–56 2014 (ICTEFAD 2014).
13. R. Yahaya, S.M. Sapuan, M. Jawaid, Z. Leman, and E.S. Zainudin, Mechanical performance of woven kenaf-Kevlar hybrid composites. *J. Reinf. Plast. Compos.* **33**(24), 2242–2254 (2014).
14. H.S. Nalwa, and R.E. Smalley, *Encyclopedia of Nanoscience and Nanotechnology*, vol. **7**, American Scientific Publishers, Valencia, CA (2004).
15. D. Harris and S. DeBolt, Relative crystallinity of plant biomass: Studies on assembly, adaptation and acclimation. *PloS One* **3**(8), e2897 (2008).
16. Z. Liu and B. Fei, Characteristics of moso bamboo with chemical pretreatment, in *Sustainable Degradation of Lignocellulosic Biomass: Techniques, Applications and Commercialization*, A.K. Chandel and S.S. da Silva (Eds.), InTech, China pp. 3–14 (2013).
17. W. Yueping, W. Ge, C. Haitao, T. Genlin, L. Zheng, X.Q. Feng, Z. Xiangqi, H. Xiaojun, and G. Xushan, Structures of natural bamboo fiber for textiles. *Text. Res. J.* **80**(4), 334–343 (2010).
18. W.L. Lai, M. Mariatti, and S.M. Jani, The properties of woven kenaf and betel palm (*Areca catechu*) reinforced unsaturated polyester composites, *Polym. Plast. Technol. Eng.* **47**(12), 1193–1199 (2008).
19. V.K. Thakur and M.K. Thakur, *Eco-friendly Polymer Nanocomposites*, Springer, New Delhi (2015).
20. P. Chua, S.R. Dai, and M.R. Piggott, Mechanical properties of the glass fibre-polyester interphase. *J. Mater. Sci.* **27**(4), 913–918 (1992).
21. H.T. Rana, Moisture diffusion through neat and glass-fiber reinforced vinyl ester resin containing nanoclay, MSc dissertation, West Virginia University, Morgantown, WV (2003).
22. A.J.F. De Carvalho, A.A.S. Curvelo, and J.A.M. Agnelli, A first insight on composites of thermoplastic starch and kaolin. *Carbohydr. Polym.* **45**(2), 189–194 (2001).
23. M.F. Huang, J.G. Yu, X.F. Ma, and P. Jin, High performance biodegradable thermoplastic starch—EMMT nanoplastics. *Polymer* **46**(9), 3157–3162 (2005).
24. S.R. Lee, H.M. Park, H. Lim, T. Kang, X. Li, W.J. Cho, and C.S. Ha, Microstructure, tensile properties, and biodegradability of aliphatic polyester/clay nanocomposites. *Polymer* **43**(8), 2495–2500 (2002).
25. M.A. Osman, J.E.P. Rupp, and U.W. Suter, Tensile properties of polyethylene-layered silicate nanocomposites. *Polymer* **46**(5), 1653–1660 (2005).
26. B.K. Behera, J. Militky, R. Mishra, and D. Kremenakova, Modeling of woven fabrics geometry and properties, in *Woven Fabrics*, H.Y. Jeon (Ed.), pp. 1–33, InTechOpen, Shanghai, China (2012).
27. D. Devaprakasam, P.V. Hatton, G. Möbus, and B.J. Inkson, Nanoscale tribology, energy dissipation and failure mechanisms of nano-and micro-silica particle-filled polymer composites. *Tribol. Lett.* **34**(1), 11–19 (2009).
28. J. Chandradass, M.R. Kumar, and R. Velmurugan, Effect of nanoclay addition on vibration properties of glass fibre reinforced vinyl ester composites. *Mater. Lett.* **61**(22), 4385–4388 (2007).
29. H.P.S. Abdul Khalil, H. Ismail, M.N. Ahmad, A. Ariffin, and K. Hassan, The effect of various anhydride modifications on mechanical properties and water absorption of oil palm empty fruit bunches reinforced polyester composites. *Polym. Int.* **50**(4), 395–402 (2001).
30. H.P.S.A. Khalil, P. Firoozian, I.O. Bakare, H.M. Akil, and A.M. Noor, Exploring biomass based carbon black as filler in epoxy composites: Flexural and thermal properties. *Mater. Design* **31(**7), 3419–3425 (2010).
31. H.G.B. Premalal, H. Ismail, and A. Baharin, Comparison of the mechanical properties of rice husk powder filled polypropylene composites with talc filled polypropylene composites. *Polym. Test.* **21(**7), 833–839 (2002).

32. V. Mortazavi, M. Atai, M. Fathi, S. Keshavarzi, N. Khalighinejad, and H. Badrian, The effect of nanoclay filler loading on the flexural strength of fiber reinforced composites. *Dent. Res. J.* **9**(3), 273–280 (2012).
33. S.Y. Fu, X.Q. Feng, B. Lauke, and Y.W. Mai, Effects of particle size, particle/matrix interface adhesion and particle loading on mechanical properties of particulate–polymer composites. *Compos. Part B-Eng.* **39**(6), 933–961 (2008).
34. S.O. Adeosun, M.A. Usman, E.I. Akpan, and W.I. Dibie, Characterization of LDPE reinforced with calcium carbonate–fly ash hybrid filler. *JMMCE* **2**, 334–345 (2014).
35. A. Alhuthali, I.M. Low, and C. Dong, Characterisation of the water absorption, mechanical and thermal properties of recycled cellulose fibre reinforced vinyl-ester eco-nanocomposites. *Compos. Part B-Eng.* **43**(7), 2772–2781 (2012).
36. L.Y. Lin, J.H. Lee, C.E. Hong, G.H. Yoo, and S.G. Advani, Preparation and characterization of layered silicate/glass fiber/epoxy hybrid nanocomposites via vacuum-assisted resin transfer molding (VARTM). *Compos. Sci. Technol.* **66**(13), 2116–2125 (2006).
37. M.N. Berhan, S. Yunus, Z. Salleh, N.R.N. Masdek, Y.M. Taib, and F.A. Ghazali, Fatigue life of kenaf woven hybrid composite. *J. Tek.* **76**(6), 37–41 (2015).
38. M.R. Loos, J. Yang, D.L. Feke, I. Manas-Zloczower, S. Unal, and U. Younes, Enhancement of fatigue life of polyurethane composites containing carbon nanotubes. *Compos. Part B-Eng.* **44**(1), 740–744 (2013).
39. S. Wicaksono and G.B. Chai, A review of advances in fatigue and life prediction of fiber-reinforced composites. *Proc. IME J. Mater. Des. Appl.* **227**(3), 179–195 (2013).
40. L. Lee, S. Rudov-Clark, A.P. Mouritz, M.K. Bannister, and I. Herszberg, Effect of weaving damage on the tensile properties of three-dimensional woven composites. *Compos. Struct.* **57**(1), 405–413 (2002).
41. L. Wang, K. Wang, L. Chen, Y. Zhang, and C. He, Preparation, morphology and thermal/mechanical properties of epoxy/nanoclay composite. *Compos. Part. A-Appl. S.* **37**(11), 1890–1896 (2006).
42. H.P.S.A. Khalil, H.M. Fizree, A.H. Bhat, M. Jawaid, and C.K. Abdullah, Development and characterization of epoxy nanocomposites based on nano-structured oil palm ash. *Compos. Part B-Eng.* **53**, 324–333 (2013).
43. R.D. dos Santos and D.M. Lenz, Biocomposites: Influence of matrix nature and additives on the properties and biodegradation behaviour in *Biodegradation - Engineering and Technology*, R. Chamy and F. Rosenkranz (Ed.), pp. 433–475, InTechOpen, Shanghai, China (2013).
44. M. Müller, H. Militz, and A. Krause, Thermal degradation of ethanolamine treated poly (vinyl chloride)/wood flour composites. *Polym. Degrad. Stab.* **97**(2), 166–169 (2012).
45. S. Lampman, *Characterization and Failure Analysis of Plastics*, ASM International, Ohio (2003).
46. M.B. Ahmad, Y. Gharayebi, M.S. Salit, M.Z. Hussein, S. Ebrahimiasl, and A. Dehzangi, Preparation, characterization and thermal degradation of polyimide (4-APS/BTDA)/SiO2 composite films. *Int. J. Mol. Sci.* **13**(4), 4860–4872 (2012).
47. M.S. Ibrahim, S.M. Sapuan, and A.A. Faieza, Mechanical and thermal properties of composites from unsaturated polyester filled with oil palm ash. *J. Mech. Eng. Sci. (JMES)* **2**, 133–147 (2012).